Ceramics International 47 (2021) 22881–22888

Contents lists available at ScienceDirect

Ceramics International

journal homepage: www.elsevier.com/locate/ceramint

Realization of high transparent conductive vanadium-doped zinc oxide thin films onto flexible PEN substrates by RF-magnetron sputtering using nanopowders targets

Samir Hamrit [a,b,*], Kamal Djessas [c,d], Kahina Medjnoun [d], Idris Bouchama [e,f], Mohammad Alam Saeed [g]

[a] Physics Department, Faculty of Sciences, Mohamed Boudiaf University - Msila, 28000, Msila, Algeria
[b] Laboratory of Materials Physics and Its Applications, University of M'sila, 28000, M'sila, Algeria
[c] Laboratoire Procédés, Matériaux et Energie Solaire (PROMES)-CNRS, Tecnosud, Rambla de la thermodynamique, 66100 Perpignan, France
[d] Université de Perpignan Via Domitia (UPVD), 52 Avenue Paul Alduy, 68860, Perpignan Cedex 9, France
[e] Electronic Department, Faculty of Technology, University Mohamed Boudiaf -Msila, 28000, Msila, Algeria
[f] Research Unit on Emerging Materials (RUEM), University of Ferhat Abbas, Setif1, 19000, Algeria
[g] Department of Physics, Division of Science & Technology, University of Education, Lahore, Pakistan

ARTICLE INFO

Keywords:
Nanopowders
RF-Magnetron sputtering
Nanostructured thin films
V-doped ZnO
PEN substrates
TCO

ABSTRACT

RF-magnetron sputtering has been carried out at room temperature to deposit vanadium-doped zinc oxide (VZO) nanostructured thin films onto flexible PEN substrates. The sputtering targets of compacted VZO nanopowder have been prepared using a rapid and inexpensive Sol-Gel synthesis followed by a supercritical drying process. Structural and morphological study of VZO particles in the targets has been carried out via X-ray diffraction and Transmission Electron Microscopy (TEM). The nanostructured thin films have been characterized to analyze the structural, morphological, electrical and optical properties as a function of vanadium content from 0 to 4 at.%. Structural characterization of VZO thin films revealed that the deposited thin films have been grown preferentially along (002) and exhibit the hexagonal wurtzite structure. The cross-sectional and microstructural analysis performed by Scanning Electron Microscopy (SEM) confirms the columnar growth of nanostructures. The deposited thin films exhibit transparent behavior with transmission >70% in the visible region. It has been observed that nanostructured thin films with vanadium content of 2% have demonstrated the lowest resistivity ($6.71 \times 10^{-4}\ \Omega$ cm) with Hall mobility of 10.62 $cm^2\ V^{-1}\ s^{-1}$. The deposited vanadium doped nanostructured thin films would have potential applications in electronic and optoelectronic devices.

1. Introduction

The development of polymer materials and significant combinatorial studies between chemistry, physics and materials sciences have revealed the possibility of using the thin flexible polymers substrates in flexible optoelectronic devices fabrication [1–6], in order to offer many advantageous characteristics such as lightness, flexibility, robustness, and can be manufactured in mass via roll-to-roll processes [7,8]. Several types of polymeric materials were used as substrates in flexible optoelectronics fabrication, including polytetrafluoroethylene (Teflon) [9], polycarbonate (PC) [10], polyethylene naphthalate (PEN) [11,12], polyethylene terephthalate (PET) [13], polyethersulfone (PES) [14] and polyimide (PI) [15]. On behalf of the optical and mechanical properties, polyethylene naphthalate (PEN) is the potential candidate among all other polymeric substrates [16].

Recently, there is an increasing demand of Transparent Conductive Oxides (TCO) with good electrical and optical properties for applications in optoelectronic devices, large area flexible displays [17] and wearable medical devices [18], solar cells [19], light-emitting diodes [14] and photovoltaic systems [20]. The most commonly used TCO in these applications is indium-tin-oxide or ITO because of its superior electrical and optical properties when compared with other TCO materials [21,22]. However, ITO has some disadvantages including its expensiveness and requirement of high temperature for deposition [23]. However, ITO thin films deposited at relatively low temperature may require further heat treatment to obtain crystalline growth which is a constraint for

* Corresponding author. Physics department, Faculty of sciences, Mohamed Boudiaf University - Msila, 28000, Msila, Algeria.
E-mail addresses: samir.hamrit1@gmail.com, samir.hamrit@univ-msila.dz (S. Hamrit).

https://doi.org/10.1016/j.ceramint.2021.04.308
Received 4 March 2021; Received in revised form 29 April 2021; Accepted 30 April 2021
Available online 13 May 2021

flexible plastic and organic substrates.

Several theoretical and experimental investigations revealed that, doped ZnO thin films as TCO when doped with suitable material can be the right replacement of ITO thin films [24,25]. Doped ZnO thin films have demonstrated many exceptional electrical and optical properties such as better electrical conductivity and optical transmittance in addition to the non-toxicity and photo stability [26,27]. Generally, post-deposition heat treatment is essential when doped ZnO thin films are deposited on variety of substrates. However, in case of organic substrates, the deposition temperature should be low enough to avoid any damaging thermal effect. DC, RF-magnetron and reactive sputtering are the well-recognized techniques to deposit doped-ZnO thin films at low temperatures [28–30]. However, the sputtering technique has some disadvantages and limitations, among them have been recently summarized by E. Stamate [31] in the introduction section. For example, the low resistivity values of sputtered TCO thin films were obtained only for limited areas of the substrate holder. This is mainly due to the negative-ions formed under the positive-ions bombardment on surfaces in low-pressure plasma. In the literature, several research has focused on resolving these problems; Lee et al. [32] have used a grid electrode between the target and the substrate to reduce the energy of negative ions originating from the target surface. Kanji Yasui et al. [33] have also used a biased grid in front of the magnetron sputtering source with a Zn target to reduce the energy of negative ions. E. Stamate also reported the possibility to improve the AZO resistivity by controlling the self-bias during RF deposition using a tuning electrode [34]. Recently, low temperature processes to deposit TCO films with low resistivity have been developed for plastic substrates, a low resistivity value of 5.45×10^{-4} Ω cm has been achieved in Al doped ZnO thin films prepared by rf magnetron without substrate heating [31]. T. Suzuki et al. [35] reported a low resistivity of 0.98 mΩ cm of VZO deposited on polycarbonate substrate.

Generally, a variety of targets were used to deposit doped zinc oxide thin films, including sintered ceramic materials, Zn and metals targets in reactive magnetron sputtering. According to literatures [36–39], the use of nanopowders targets in the sputtering technique is an excellent route to realizing nanostructured thin films with better electrical and optical properties. Nuno Neves et al. [40] reported that the electrical properties of films deposited by rf magnetron sputtering under the same conditions are strongly influenced by the properties of the starting powder, and consequently by the target properties. Bouznit et al. [41] reported the effect of the target nature on the properties of the deposited Al doped ZO thin films prepared by RF magnetron sputtering at room temperature. They have proven that the films deposited from nanopowders targets are transparent and have a better electrical conductivity than the films deposited from ceramic targets. It has also been established that the role of starting material (target) in RF-magnetron sputtering is very much important to realize thin films with high optoelectronic properties. To the best of our knowledge, the reports on the properties of V doped ZnO thin films deposited on flexible PEN substrates by rf-magnetron sputtering using a nanopowder targets of VZO prepared by the sol-gel process combined with supercritical drying process are scarce up to now.

In the current study, VZO aerogel nanoparticles have been used to deposit nanostructured VZO thin films on PEN substrates by RF-magnetron sputtering without intentional heating of the substrate. The structural, morphological, electrical and optical characterizations were carried out to investigate the effect of vanadium content and viability of potential transparent electrode. Four samples with vanadium content from 1 to 4 at.% have been prepared using the combination of Sol-Gel and supercritical drying process. The sputtering targets were prepared without host-pressing or sintering at higher temperatures.

2. Experimental details

The overall experiment was carried out in two steps i.e., synthesis of nanopowders via Sol-Gel method followed by deposition of thin films via RF-magnetron sputtering. For the synthesis of nanopowders, zinc acetate dihydrate and ammonium metavanadate were used as starting material, however, methanol was used as solvent. The Sol-Gel synthesis was started by dissolving the zinc acetate dihydrate in methanol under vigorous stirring at room temperature for 20 min. Afterwards, an appropriate amount of ammonium metavanadate was added corresponding to obtain the vanadium concentration varying from 1 to 4% in the final solution. After 20 min of vigorous stirring, clear and transparent solutions were obtained which were then transferred to an autoclave and dried in supercritical conditions. The VZO aerogels collected from the autoclave were annealed in ambient conditions for 2 h at 500 °C. The annealed powders were then pressed mechanically to obtain pellets of 50 mm diameter.

Flexible Polyethylene Naphtalate (PEN) substrate were selected for the deposition of nanostructured thin films from VZO compacted nanopowder targets by RF-magnetron sputtering. The samples were deposited based on the optimized working parameters of sputtering that are as follows; sputtering chamber pressure $<10^{-5}$ mbar, working pressure 10^{-3} mbar, RF power 60 W, distance between substrate and target 7 cm.

Poly-Ethylene Naphtalate (PEN) samples of 15 × 20 mm and 0.75 μm of thickness obtained from Goodfellow Cambridge Limited Huntingdon PE29 6WR was cleaned prior to deposition in an ultrasonic bath containing ethyl alcohol, and then placed on a large holder of 10 cm in diameter. Then since the substrate being used was a polymer, so there is no heat treatment involved prior to sputtering. However, within the sputtering chamber, the temperature of the substrate may rise up to 75 °C due to involvement of high energy particles.

The crystalline and structure of nanopowder was characterized by X-ray diffraction (XRD) and Transmission Electron Microscope (TEM). For XRD analysis, Bruker D8 discover diffractometer with Cu target Kα lines and for TEM analysis, JEOL 100C microscope operating at an acceleration voltage of 100 kV, were used. The cross-section of the thin films was taken of the cleaved samples by using Scanning Electron Microscope (SEM, HITACHI S4500). The atomic percent (at%) of V, Zn and O elements in the VZO thin films was analyzed by Energy Dispersive Spectroscopy (EDS) attached to the Hitachi SEM S4500. Room-temperature Hall effect measurements were carried out using an Ecopia HMS-3000 Hall effect measurement system with a magnetic field of 0.56 T. The photoluminescence (PL) spectra were recorded at room-temperature using a PerkinElmer (LS-50B) luminescence spectrometer with a Xenon lamp as excitation source (325 nm). Transmittance measurements were carried out by UV/Vis/NIR VARIAN Cary 5000 Spectrophotometer in the wavelength range from 180 to 3300 nm.

3. Results and discussion

3.1. Samples characterization (nano powders)

Fig. 1 shows the X-ray diffraction patterns of V-doped zinc oxide nanopowder samples. The observed diffraction peaks correspond to hexagonal wurtzite structure of ZnO in accordance with the JCPDS data (No. 36–1451). All the samples did not exhibit any diffraction peak related to V_2O_5 or other phases validating the absence of any secondary phases.

Fig. 2 shows the typical TEM image of the V-doped ZnO at vanadium concentration of 2%. The observed morphology of the particles in nanopowder is roughly spherical and the average size of these particles ranges from 30 to 40 nm.

3.2. Sample characterization (thin films)

3.2.1. Structural analysis

Fig. 3 shows the X-ray diffraction patterns of sputtered VZO thin films. All the diffraction patterns exhibit the diffraction peaks corresponding to ZnO and the substrate. The diffraction peaks observed at 2θ

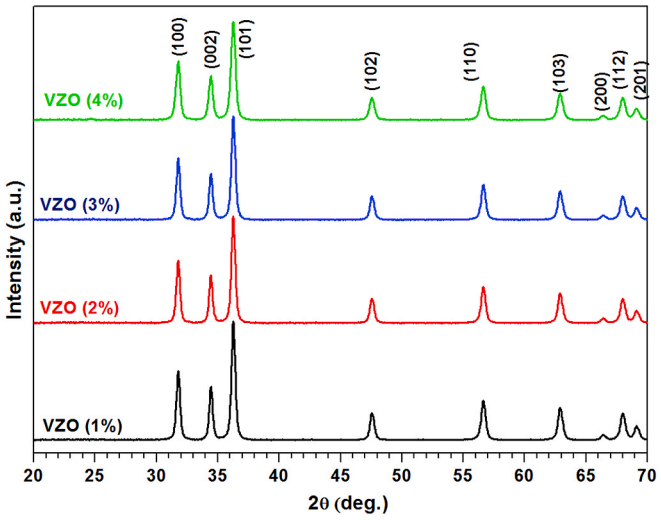

Fig. 1. X-ray diffraction patterns of V-doped zinc oxide nanopowders samples.

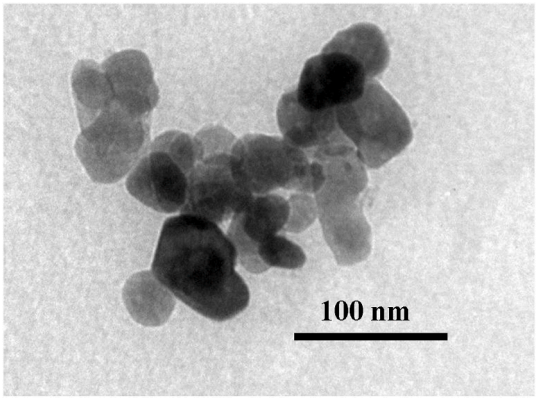

Fig. 2. TEM image of V-doped ZnO nanopowder with 2 at.% of V concentration.

values of 26.91° and 55.86° correspond to the PEN substrate [36]. The existence of diffraction peak at 2θ value of 34.36° correspond to the (002) plane in all the samples and depict the preferential growth of ZnO on to the substrate surface with hexagonal wurtzite structure. The XRD data obtained for all the vanadium doped samples is consistent with standard card (JCPDS 36–1451). The origin of the preferred orientation of V-doped ZnO films is due to the existence of minimal surface energy and polar nature of the host material along (002) plane in addition to the high growth kinetics in the direction of *c*-axis [42].The crystallinity of the deposited thin films is evident from the systematic narrowing of Full Width at Half Maximum (FWHM).

From XRD patterns, it has been observed that the intensity of diffraction peaks decreases as a function of dopant concentration. Particularly, the intensity of most prominent diffraction peak corresponding to the (002) plane is observed to be lowered at dopant concentration of 3 and 4 at.%. This decrement in intensity of diffraction peak might be due to solid solubility limit of the host material for the vanadium dopant.

The lattice parameters *c* and the interplanar spacing $d_{(002)}$ of VZO films were calculated using the following equations [43,44]:

$$n\lambda = 2d_{hkl}sin\theta \tag{1}$$

$$d_{hkl} = \frac{a}{\sqrt{\frac{4}{3}\left(h^2 + k^2 + hk\right) + \frac{a^2}{c^2}l^2}} \tag{2}$$

Where *d* is the interplanar spacing which can be obtained from Bragg's law, *h*, *k* and *l* are the Miller indices denoting the plane, λ is the X-ray wavelength ($\lambda = 1.5418$Å) and θ is the diffraction angle.

For the first order approximation, $n = 1$.

$$c = \frac{\lambda}{2sin\theta}\sqrt{\frac{4c^2}{3a^2}\left(h^2 + hk + l^2\right)} \tag{3}$$

For the (002) orientation, the lattice constant *c* was:

$$c = \frac{\lambda}{sin\theta} \tag{4}$$

The average crystallite size in the VZO films was calculated using Debye–Scherrer's formula [45]:

$$D = \frac{0.9\lambda}{\beta cos\theta} \tag{5}$$

Where *D* is the crystallite size (nm), λ is the X-ray wavelength (λ = 1.5418 Å), β is the full width at half maximum, and θ is the diffraction angle. The interreticular distance $d_{(002)}$, peak position (002), FWHM, average crystallite size, lattice parameters *c*, obtained from the XRD data for the VZO thin films are summarized in Table 1.

It is clear from Table 1 that the crystallite size *D* and the lattice parameter *c* are increased, as the V dopant concentration increases in ZnO lattice. This variation would probably result from: (1) An increased incorporation of V atoms in the interstitial sites of ZnO lattice (2) free-electron concentration acting via deformation potential of a conduction-band minimum occupied by these electrons [46], (3) external strains, for example, those induced by substrate and temperature.

Fig. 4 presents the cross-sectional micrograph of the doped sample with 2 at.% of vanadium concentration taken from Scanning Electron Microscopic (SEM). A very dense columnar growth of nanostructures along the *c*-axis validates the XRD data. The thickness of the VZO film with 2 at.% of vanadium is observed to be around 450 nm.

Energy Dispersive X-ray (EDX) Spectroscopy was utilized to access the chemical composition of the VZO thin films grown on PEN substrates. Fig. 5 depicted that sole presence of peaks related to zinc (Zn), oxygen (O) and vanadium (V) atoms, indicating high purity of the grown VZO thin films within the detection limit. The deposited VZO thin films exhibit no evidence for the existence contaminants and impurities in the samples.

3.2.2. *Electrical properties*

Fig. 6 shows the specific electrical properties of VZO thin films deposited on PEN substrates like resistivity, mobility, and carrier concentration as a function of dopant concentration, the measurement was carried on 5 × 5 mm^2 of samples. The carrier concentration is observed to increase after vanadium incorporation in ZnO host lattice and attain a maximum value of 10.13 × $10^{20}cm^{-3}$ when the dopant concentration is 3 at.%. Afterwards, the carrier concentration was observed to decrease and has a value of 7.11 × 10^{20} cm^{-3} for maximum concentration of dopant i.e. 4 at.%. This variation in carrier concentration of VZO thin films can be explained in terms of solid solubility limit of ZnO lattice. At low doping concentrations, the V ions contribute towards adding the electrons in conduction band. However, at higher dopant concentration, the vanadium atoms act as an electron trap and ultimately decrease the carrier concentration. The resistivity has its lowest value of 6.71 × 10^{-4} Ω cm for VZO thin films with vanadium concentration of 2 at.% and has its maximum value of 3.83 × 10^{-3} Ω cm for VZO thin films with vanadium concentration of 4 at.%. The Hall mobility shows decreasing behavior with increasing vanadium concentrations and reaches a minimum value of 2.28 cm^2 V^{-1} s^{-1}, its maximum value is 10.62 cm^2 V^{-1} s^{-1} for the vanadium concentration 2 at.%. The carrier mobility is influenced by multiple scattering mechanisms, such as the grain

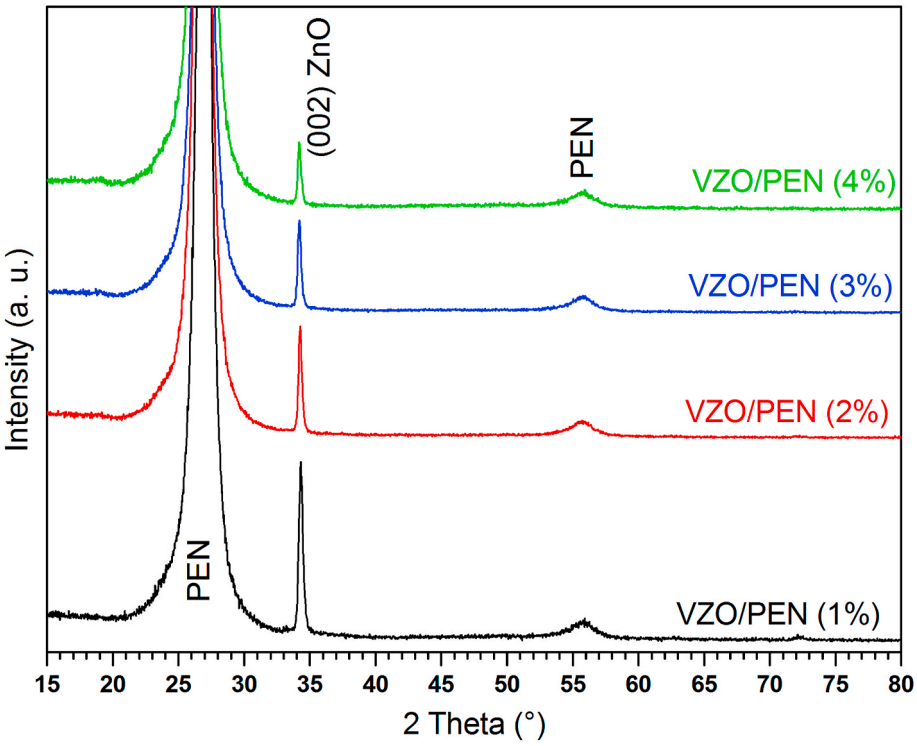

Fig. 3. X-ray diffraction patterns of VZO thin films on PEN substrate with different V concentrations.

Table 1
Structural parameters of VZO thin films on PEN substrate with different V concentrations.

Sample	2θ(002)	FWHM	Average grain size (nm)	$d_{(002)}$ (Å)	c(Å)
VZO (1%)	34.31	0.382	~22	2.614	5.227
VZO (2%)	34.26	0.321	~26	2.618	5.237
VZO (3%)	34.20	0.327	~27	2.623	5.246
VZO (4%)	34.20	0.317	~28	2.623	5.246

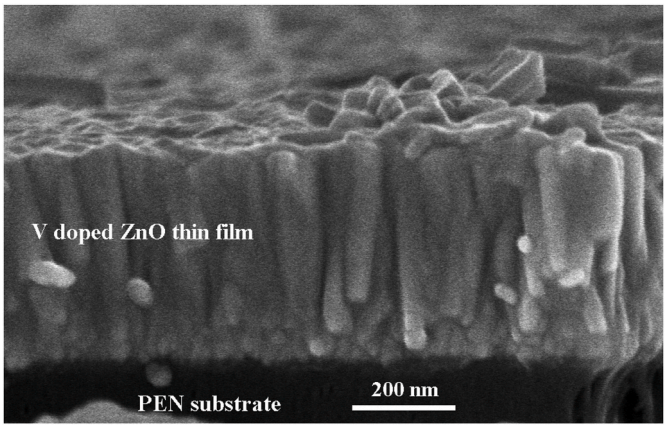

Fig. 4. Cross-section SEM image of V-doped ZnO (2 at.%) thin film on PEN substrate.

boundary scattering, the ionized impurity scattering and the neutral impurity scattering. The increase of V content in the ZnO could contribute to produce the free electron carriers, simultaneously it causes a decrease in the carrier mobility by forming the ionized impurity scattering centers to trap the free electron carriers.

3.2.3. Optical properties

Fig. 7 depicts the room temperature photoluminescence (PL) spectrum of VZO thin films grown on PEN substrate with 2 at.% of V content. As can be illustrated in the figure, the spectrum of sample could be deconvoluted into five Gaussian emissions peaks, i.e. UV emission at 383.5 nm (3.23 eV) corresponding to the near-band edge emission of ZnO [47], three blue emission at 411 nm (3.01 eV), 426 nm (2.91 eV) and 472.5 (2.62 eV) originated from polymer [36] and surface defects in the ZnO nanostructures, such as oxygen vacancies (V_0) and Zn interstitial (Zn_i) [47] and green emission at 518 nm (2.39 eV) results to the point defects related to the surface such as antisite oxygen O_{Zn} according to the calculations energy levels of the defects in ZnO films by Xu et al. [48]. It is well known that; UV is the main emission in the ZnO thin films that corresponds to the exciton recombination due to the annihilation process [49]. However, the possible reason for the appearance of strong blue emissions would be that the surface defects of oxygen vacancies (V_O) and Zn interstitial (Zn_i) are more dominant than the other defects in the prepared VZO thin film.

The transmission spectra in the wavelength range from 300 to 2000 nm for the VZO thin films deposited on the PEN substrates are shown in Fig. 8. The Transmittance was measured at room temperature, using PEN substrate as a reference. All the sputtered VZO films exhibit an average optical transmittance higher than 70% in the spectral range from 400-1200 nm.

In the near infrared (NIR) region, the transmittance decreases for all the V-doped ZnO thin films. This change of the optical properties may be caused by free carriers' absorption, the so-called plasmonic absorption, which can be understood on the basis of the Drude model [50].

$$\alpha = \frac{ne^2\lambda^2}{m^* 8\pi^2 N c_0^3 \tau} \tag{8}$$

Where α, n, m^*, N, and τ represent are the optical absorption coefficient, effective mass, refractive index, and the carrier relaxation time, respectively. Higher the carrier concentration, more will be the absorption in the longer wavelength region.

In the UV range, all the VZO thin films exhibited a sharp absorption

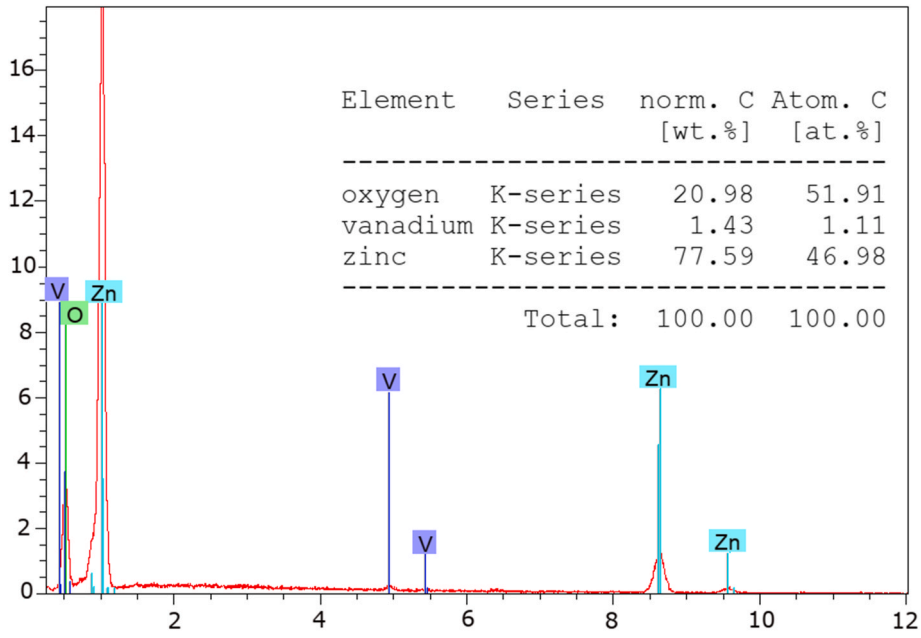

Fig. 5. EDS spectrum and atomic percentage of elements composition in V-doped ZnO thin films with 2 at.% of V content.

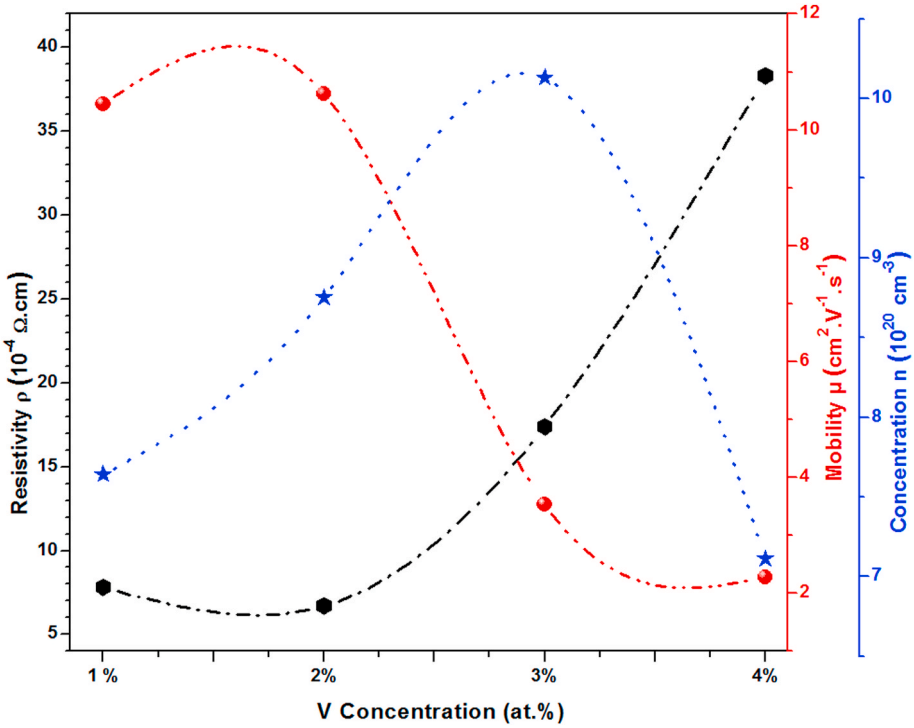

Fig. 6. Resistivity, Hall mobility and carrier concentration of V-doped ZnO thin films on PEN substrate with different V concentrations.

edge and is observed to be shifted slightly towards the shorter wavelength as a function of dopant's concentration. This movement of the absorption edge can be explained by the Burstein-Moss effect [51], which is closely related to the free carrier density in conduction band. The blue shift of absorption edge is the result of an increase in the carrier concentrations.

4. Conclusion

VZO nanostructured thin films as a TCO material have been deposited on PEN flexible substrate using compacted VZO nanopowders via RF-magnetron Sputtering. The investigations of structural, morphological, electrical and optical properties of VZO thin films help to speculate an optimal vanadium concentration for VZO thin films in order to achieve the high quality TCO. The VZO films with 2 at.% of vanadium exhibited a low resistivity of 6.71×10^{-4} Ω cm, Hall mobility of 10.62 $cm^2\ V^{-1}\ s^{-1}$ and a high transmittance >75% in the visible region. These TCO thin films can have potential to be used in flexible electronic applications such as solar cells.

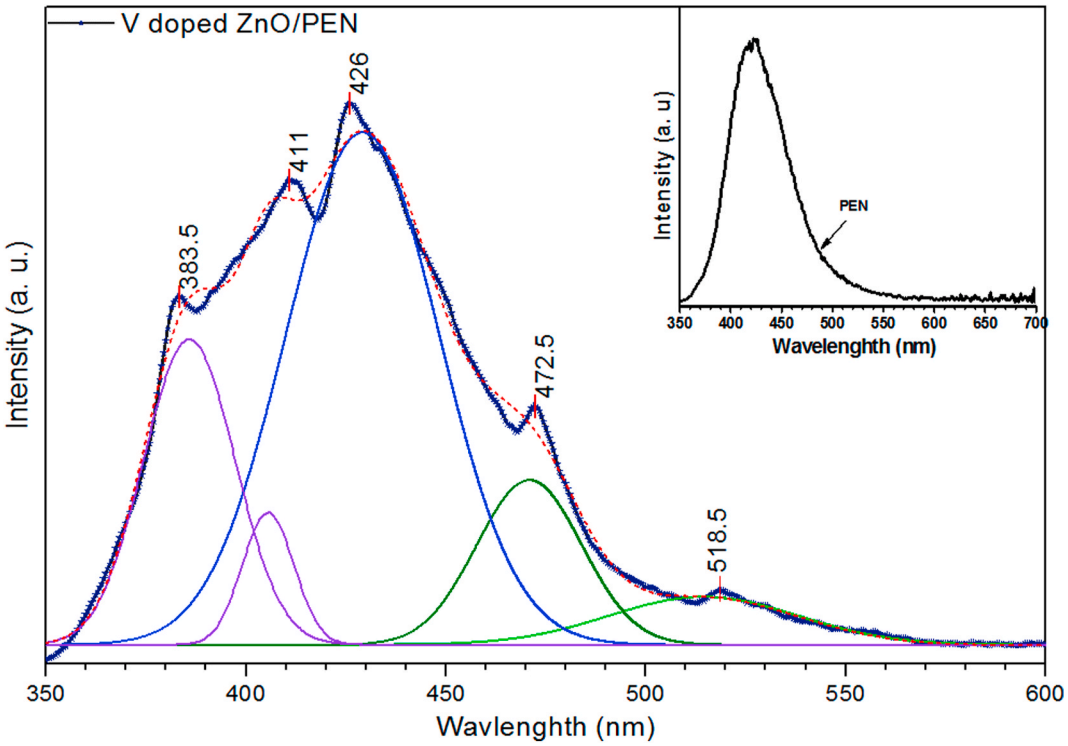

Fig. 7. Room temperature photoluminescence spectrum of VZO (2 at.%)/PEN sample.

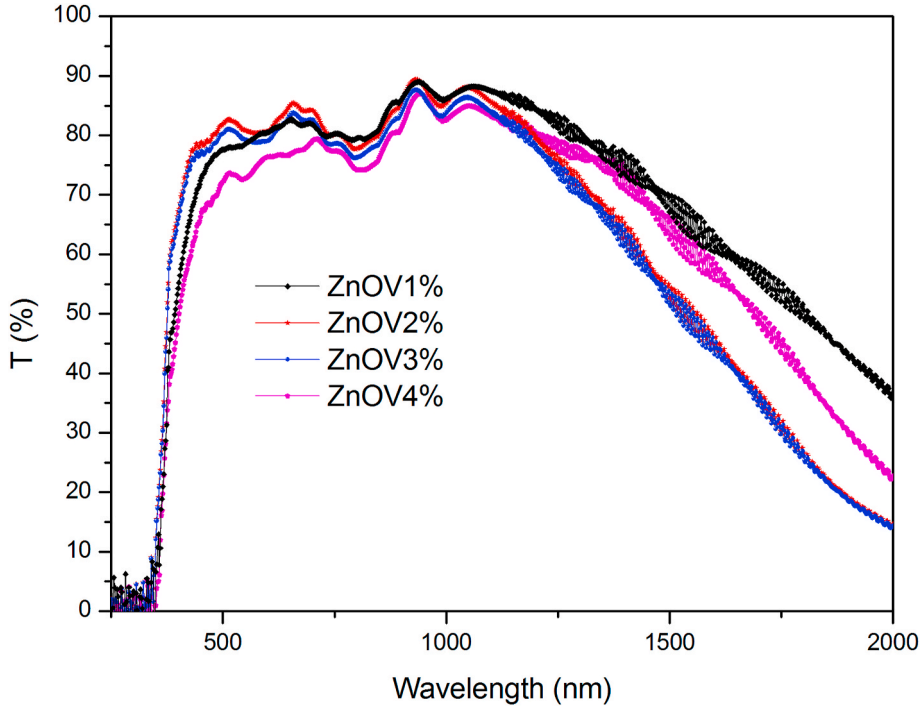

Fig. 8. Optical transmittance spectra of VZO thin films deposited on PEN substrate with different Al concentrations.

Declaration of competing interest

The authors declare that they have no known competing financial interests or personal relationships that could have appeared to influence the work reported in this paper.

Acknowledgements

The authors would like to thank J. L. Gauffier and S. Reyjal (Department of Physics and Engineering, INSA-Toulouse, France) for TEM and EDX measurements.

References

[1] F. Machda, T. Ogawa, H. Okumura, K.N. Ishihara, Damp-heat durability comparison of Al-doped ZnO transparent electrodes deposited at low temperatures on glass and PI-tape/PC substrates, Ceram. Int. 46 (2020) 16178–16184, https://doi.org/10.1016/j.ceramint.2020.03.173.

[2] H.C. Weerasinghe, F. Huang, Y.-B. Cheng, Fabrication of flexible dye sensitized solar cells on plastic substrates, Nanomater. Energy 2 (2013) 174–189, https://doi.org/10.1016/j.nanoen.2012.10.004.

[3] Z. Jiang, F. Wang, K. Fukuda, A. Karki, W. Huang, K. Yu, et al., Highly efficient organic photovoltaics with enhanced stability through the formation of doping-induced stable interfaces, Proc. Natl. Acad. Sci. U.S.A. 117 (2020) 6391–6397, https://doi.org/10.1073/pnas.1919769117.

[4] S. Park, S.W. Heo, W. Lee, D. Inoue, Z. Jiang, K. Yu, et al., Self-powered ultra-flexible electronics via nano-grating-patterned organic photovoltaics, Nature 561 (2018) 516–521, https://doi.org/10.1038/s41586-018-0536-x.

[5] F.F. Vidor, T. Meyers, U. Hilleringmann, Flexible electronics: integration processes for organic and inorganic semiconductor-based thin-film transistors, Electronics 4 (2015) 480–506, https://doi.org/10.3390/electronics4030480.

[6] W. A MacDonald, M.K. Looney, D. MacKerron, R. Eveson, R. Adam, K. Hashimoto, et al., Latest advances in substrates for flexible electronics, J. Soc. Inf. Disp. 15 (2007) 1075–1083, https://doi.org/10.1889/1.2825093.

[7] M. Yano, K. Suzuki, K. Nakatani, H. Okaniwa, Roll-to-roll preparation of a hydrogenated amorphous silicon solar cell on a polymer substrate, Thin Solid Films 146 (1987) 75–81, https://doi.org/10.1016/0040-6090(87)90341-5.

[8] M. Izu, T. Ellison, Roll-to-roll manufacturing of amorphous silicon alloy solar cells with in situ cell performance diagnostics, Sol. Energy Mater. Sol. Cells 78 (2003) 613–626, https://doi.org/10.1016/S0927-0248(02)00454-3.

[9] Y. Liu, Y. Yuan, C. Li, X. Gao, X. Cao, J. Li, The structure and photoluminescence properties of RF-sputtered films of ZnO on Teflon substrate, Mater. Lett. 62 (2008) 2907–2909, https://doi.org/10.1016/j.matlet.2008.01.070.

[10] L. Sowntharya, S. Lavanya, G.R. Chandra, N.Y. Hebalkar, R. Subasri, Investigations on the mechanical properties of hybrid nanocomposite hard coatings on polycarbonate, Ceram. Int. 38 (2012) 4221–4228, https://doi.org/10.1016/j.ceramint.2012.01.081.

[11] K. Kinoshita, T. Okutani, H. Tanaka, T. Hinoki, H. Agura, K. Yazawa, et al., Flexible and transparent ReRAM with GZO memory layer and GZO-electrodes on large PEN sheet, Solid State Electron. 58 (2011) 48–53, https://doi.org/10.1016/j.sse.2010.11.026.

[12] M. Fonrodona, J. Escarre, F. Villar, D. Soler, J. Asensi, J. Bertomeu, et al., PEN as substrate for new solar cell technologies, Sol. Energy Mater. Sol. Cells 89 (2005) 37–47, https://doi.org/10.1016/j.solmat.2004.12.006.

[13] M. Mikula, P. Gemeiner, Z. Beková, V. Dvonka, D. Búc, Dye-sensitized solar cells based on different nano-oxides on plastic PET substrate, J. Phys. Chem. Solids. 76 (2015) 17–21, https://doi.org/10.1016/j.jpcs.2014.07.020.

[14] P.H. Lei, C.M. Hsu, Y.S. Fan, Flexible organic light-emitting diodes on a polyestersulfone (PES) substrate using Al-doped ZnO anode grown by dual-plasma-enhanced metalorganic deposition system, Org. Electron. 14 (2013) 236–249, https://doi.org/10.1016/j.orgel.2012.10.030.

[15] T.-R. Rashid, D.-T. Phan, G.-S. Chung, A flexible hydrogen sensor based on Pd nanoparticles decorated ZnO nanorods grown on polyimide tape, Sensor. Actuator. B Chem. 185 (2013) 777–784, https://doi.org/10.1016/j.snb.2013.01.015.

[16] E.L. Bedia, S. Murakami, T. Kitade, S. Kohjiya, Structural development and mechanical properties of polyethylene naphthalate/polyethylene terephthalate blends during uniaxial drawing, Polymer 42 (2001) 7299–7305, https://doi.org/10.1016/S0032-3861(01)00236-1.

[17] U. Betz, M. Kharrazi Olsson, J. Marthy, M.F. Escolá, F. Atamny, Thin films engineering of indium tin oxide: large area flat panel displays application, Surf. Coating. Technol. 200 (2006) 5751–5759, https://doi.org/10.1016/j.surfcoat.2005.08.144.

[18] K. Sim, Z. Rao, Z. Zou, F. Ershad, J. Lei, A. Thukral, et al., Metal oxide semiconductor nanomembrane–based soft unnoticeable multifunctional electronics for wearable human-machine interfaces, Sci. Adv. 5 (2019) 1–11, https://doi.org/10.1126/sciadv.aav9653.

[19] K. Ellmer, A. Klein, B. Rech, Transparent conductive zinc oxide. Basics and Applications in Thin Film Solar Cells, 2008, https://doi.org/10.1007/978-3-540-73612-7_5.

[20] E. Pulli, E. Rozzi, F. Bella, Transparent photovoltaic technologies: current trends towards upscaling, Energy Convers. Manag. 219 (2020) 112982, https://doi.org/10.1016/j.enconman.2020.112982.

[21] T. Minami, Present status of transparent conducting oxide thin-film development for Indium-Tin-Oxide (ITO) substitutes, Thin Solid Films 516 (2008) 5822–5828, https://doi.org/10.1016/j.tsf.2007.10.063.

[22] E.B. Aydın, M.K. Sezgintürk, Indium tin oxide (ITO): a promising material in biosensing technology, TrAC Trends Anal. Chem. (Reference Ed.) 97 (2017) 309–315, https://doi.org/10.1016/j.trac.2017.09.021.

[23] S. Marikkannu, M. Kashif, N. Sethupathy, V.S. Vidhya, S. Piraman, a. Ayeshamariam, et al., Effect of substrate temperature on indium tin oxide (ITO) thin films deposited by jet nebulizer spray pyrolysis and solar cell application, Mater. Sci. Semicond. Process. 27 (2014) 562–568, https://doi.org/10.1016/j.mssp.2014.07.036.

[24] F.X. Jiang, R.X. Tong, Z. Yan, L.F. Ji, X.H. Xu, d-electron-dependent transparent conducting oxide of V-doped ZnO thin films, J. Alloys Compd. 822 (2020) 153706, https://doi.org/10.1016/j.jallcom.2020.153706.

[25] J.S. Jang, J. Kim, U. Ghorpade, H.H. Shin, M.G. Gang, S.D. Park, et al., Comparison study of ZnO-based quaternary TCO materials for photovoltaic application, J. Alloys Compd. 793 (2019) 499–504, https://doi.org/10.1016/j.jallcom.2019.04.042.

[26] J.I. Nomoto, Y. Nishi, T. Miyata, T. Minami, Influence of the kind and content of doped impurities on impurity-doped ZnO transparent electrode applications in thin-film solar cells, Thin Solid Films 534 (2013) 426–431, https://doi.org/10.1016/j.tsf.2012.07.141.

[27] K. Jung, W.-K. Choi, K.H. Chae, J.-H. Song, S.-J. Yoon, M.-H. Lee, et al., Highly conductive and damp heat stable transparent ZnO based thin films for flexible electronics, J. Alloys Compd. 554 (2013) 240–245, https://doi.org/10.1016/j.jallcom.2012.11.021.

[28] Z. Ben Ayadi, L. El Mir, K. Djessas, S. Alaya, Effect of the annealing temperature on transparency and conductivity of ZnO:Al thin films, Thin Solid Films 517 (2009) 6305–6309, https://doi.org/10.1016/j.tsf.2009.02.062.

[29] X. Zhang, L. Zhu, H. Xu, L. Chen, Y. Guo, Z. Ye, Highly transparent conductive F-doped ZnO films in wide range of visible and near infrared wavelength deposited on polycarbonate substrates, J. Alloys Compd. 614 (2014) 71–74, https://doi.org/10.1016/j.jallcom.2014.06.098.

[30] L. Wen, M. Kumar, B.B. Sahu, S.B. Jin, C. Sawangrat, K. Leksakul, et al., Advantage of dual-con fi ned plasmas over conventional and facing-target plasmas for improving transparent-conductive properties in Al doped ZnO thin fi lms, Surf. Coating. Technol. 284 (2015) 85–89, https://doi.org/10.1016/j.surfcoat.2015.06.084.

[31] E. Stamate, Spatially resolved optoelectronic properties of aldoped zinc oxide thin films deposited by radiofrequency magnetron plasma sputtering without substrate heating, Nanomaterials 10 (2020) 1–11, https://doi.org/10.3390/nano10010014.

[32] H.N. Lee, J.Y. Hur, H.J. Kim, M.H. Lee, H.K. Lee, Indium tin oxide films with low resistivity at room temperature using dc magnetron sputtering with grid electrode, Mater. Trans. 55 (2014) 605–609, https://doi.org/10.2320/matertrans.M2013316.

[33] K. Yasui, N.V. Phuong, Y. Kuroki, M. Takata, T. Akahane, Improvement in crystallinity of ZnO films prepared by rf magnetron sputtering with grid electrode, Japanese J. Appl. Physics, Part 1 Regul, Pap. Short Notes Rev. Pap. 44 (2005) 684–687, https://doi.org/10.1143/JJAP.44.684.

[34] E. Stamate, Lowering the resistivity of aluminum doped zinc oxide thin films by controlling the self-bias during RF magnetron sputtering, Surf. Coating. Technol. 402 (2020) 126306, https://doi.org/10.1016/j.surfcoat.2020.126306.

[35] T. Suzuki, H. Chiba, T. Kawashima, K. Washio, Comparison study of V-doped ZnO thin films on polycarbonate and quartz substrates deposited by RF magnetron sputtering, Thin Solid Films 605 (2016) 53–56, https://doi.org/10.1016/j.tsf.2015.11.064.

[36] S. Hamrit, K. Djessas, N. Brihi, B. Viallet, K. Medjnoun, S.E. Grillo, The effect of thickness on the physico-chemical properties of nanostructured ZnO : Al TCO thin fi lms deposited on fl exible PEN substrates by RF-magnetron sputtering from a nanopowder target, Ceram. Int. 42 (2016) 16212–16219, https://doi.org/10.1016/j.ceramint.2016.07.143.

[37] K.H. Kim, R.A. Wibowo, B. Munir, Properties of Al-doped ZnO thin film sputtered from powder compacted target, Mater. Lett. 60 (2006) 1931–1935, https://doi.org/10.1016/j.matlet.2005.12.055.

[38] S. Hamrit, K. Djessas, N. Brihi, O. Briot, M. Moret, Z. Ben Ayadi, Study and optimization of Al-doped ZnO thin films deposited on PEN substrates by RF-magnetron sputtering from nanopowders targets, J. Mater. Sci. Mater. Electron. 27 (2016) 1730–1737, https://doi.org/10.1007/s10854-015-3947-6.

[39] Z. Ben Ayadi, L. El Mir, K. Djessas, S. Alaya, Electrical and optical properties of aluminum-doped zinc oxide sputtered from an aerogel nanopowder target, Nanotechnology 18 (2007) 445702, https://doi.org/10.1088/0957-4484/18/44/445702.

[40] N. Neves, R. Barros, E. Antunes, I. Ferreira, J. Calado, E. Fortunato, et al., Sintering behavior of nano- and micro-sized ZnO powder targets for rf magnetron sputtering applications, J. Am. Ceram. Soc. 95 (2012) 204–210, https://doi.org/10.1111/j.1551-2916.2011.04874.x.

[41] Y. Bouznit, Y. Beggah, K. Djessas, RF magnetron sputtering of ZnO and Al-doped ZnO films from ceramic and nanopowder targets: a comparative study, J. Sol. Gel Sci. Technol. 61 (2012) 449–454, https://doi.org/10.1007/s10971-011-2645-y.

[42] Y. Kajikawa, Texture development of non-epitaxial polycrystalline ZnO films, J. Cryst. Growth 289 (2006) 387–394, https://doi.org/10.1016/j.jcrysgro.2005.11.089.

[43] O. Lupan, T. Pauporté, L. Chow, B. Viana, F. Pellé, L.K. Ono, et al., Effects of annealing on properties of ZnO thin films prepared by electrochemical deposition in chloride medium, Appl. Surf. Sci. 256 (2010) 1895–1907, https://doi.org/10.1016/j.apsusc.2009.10.032.

[44] C.H. Ahn, S.Y. Lee, H.K. Cho, Influence of growth temperature on the electrical and structural characteristics of conductive Al-doped ZnO thin films grown by atomic layer deposition, Thin Solid Films 545 (2013) 106–110, https://doi.org/10.1016/j.tsf.2013.07.045.

[45] S. Benramache, H. Ben Temam, A. Arif, A. Guettaf, O. Belahssen, Correlation between the structural and optical properties of Co doped ZnO thin films prepared at different film thickness, Opt. - Int. J. Light Electron Opt. 125 (2014) 1816–1820, https://doi.org/10.1016/j.ijleo.2013.09.024.

[46] Ü. Özgür, Y.I. Alivov, C. Liu, A. Teke, M.A. Reshchikov, S. Doğan, et al., A comprehensive review of ZnO materials and devices, J. Appl. Phys. 98 (2005) 1–103, https://doi.org/10.1063/1.1992666.

[47] N.S. Sabri, A.K. Yahya, M.K. Talari, Emission properties of Mn doped ZnO nanoparticles prepared by mechanochemical processing, J. Lumin. 132 (2012) 1735–1739, https://doi.org/10.1016/j.jlumin.2012.02.020.

[48] P.S. Xu, Y.M. Sun, C.S. Shi, F.Q. Xu, H.B. Pan, The electronic structure and spectral properties of ZnO and its defects, Nucl. Instrum. Methods Phys. Res. Sect. B Beam

Interact. Mater. Atoms 199 (2003) 286–290, https://doi.org/10.1016/S0168-583X(02)01425-8.

[49] P. Chand, A. Gaur, A. Kumar, U.K. Gaur, Structural, morphological and optical study of Li doped ZnO thin films on Si (100) substrate deposited by pulsed laser deposition, Ceram. Int. 40 (2014) 11915–11923, https://doi.org/10.1016/j.ceramint.2014.04.027.

[50] M.M. Islam, S. Ishizuka, A. Yamada, K. Matsubara, S. Niki, T. Sakurai, et al., Thickness study of Al:ZnO film for application as a window layer in Cu(In1−xGax)Se2 thin film solar cell, Appl. Surf. Sci. 257 (2011) 4026–4030, https://doi.org/10.1016/j.apsusc.2010.11.169.

[51] E. Burstein, Anomalous optical absorption limit in InSb [4], Phys. Rev. 93 (1954) 632–633, https://doi.org/10.1103/PhysRev.93.632.